

Comparison of Observed and Synthetic Dynamic Ground Strains and Rotations in the Near-Fault Region of the 2004 Parkfield Earthquake



UNIVERSITY OF
NOTRE DAME

Yenan Cao¹, George P. Mavroeidis¹, and Mansoor Ashoory²

¹ Department of Civil and Environmental Engineering and Earth Sciences, University of Notre Dame, Notre Dame, IN 46556

² Department of Civil Engineering, The Catholic University of America, Washington, DC 20064

THE CATHOLIC
UNIVERSITY
OF AMERICA

1. Abstract

Several studies have generated low-frequency dynamic ground deformations (strains and rotations) in the near-fault region of actual or hypothetical earthquakes using physics-based simulation techniques. However, no systematic attempt has been made to compare observed and synthetic near-fault dynamic ground strains and rotations in order to demonstrate the effectiveness of the simulation techniques in predicting these motions. Such a comparison is presented in this study for the 2004 M_w 6.0 Parkfield, California, earthquake, which occurred on the San Andreas fault and was recorded by a dense network of instruments. Following the work of Spudich and Fletcher (2008), estimates of near-fault dynamic ground strains and rotations are obtained by applying time-dependent geodetic analysis to displacement time histories recorded by the U.S. Geological Survey Parkfield Seismic Array (UPSA) and Turkey Flat array. A forward ground-motion simulation of the 2004 Parkfield earthquake is performed using the fault and crustal models proposed by Liu et al. (2006), and low-frequency translational motions, strains, and rotations are generated at selected stations. The computations are carried out using the discrete wavenumber representation method and the generalized transmission and reflection coefficient technique. The synthetic motions are generally in good agreement with the recorded translational motions, the recorded borehole volumetric strains, the array-derived strains and rotations, and the finite-difference approximated displacement gradients in both time and frequency domains. The results indicate that numerical simulations based on kinematic source models can be an effective tool for characterizing and predicting low-frequency dynamic ground deformations in the near-fault region. However, further research is necessary to explore whether simulation approaches based on classical linear elasticity theory are sufficient to predict near-fault dynamic ground strains and rotations from major earthquakes. In addition, the effect of lateral heterogeneities, nonlinear soil response, ground failure, and soil liquefaction on dynamic ground deformations should also be investigated.

2. Instrumentation and Data

Ground motions in the near-fault region of the 2004 Parkfield earthquake were recorded by an extensive set of strong-motion instruments. The acceleration and volumetric strain data obtained at the Donna Lee, Froelich, and Vineyard Canyon sites of the U.S. Geological Survey (USGS) General Earthquake Observation System (GEOS) array are used in this study. The surface accelerometers at the three sites are denoted as stations DFU, FFU, and VFU, whereas the co-located borehole volumetric strainmeters are denoted as stations DLD, FRD, and VCD. Ground motions from the UPSAR and Turkey Flat array are also used.

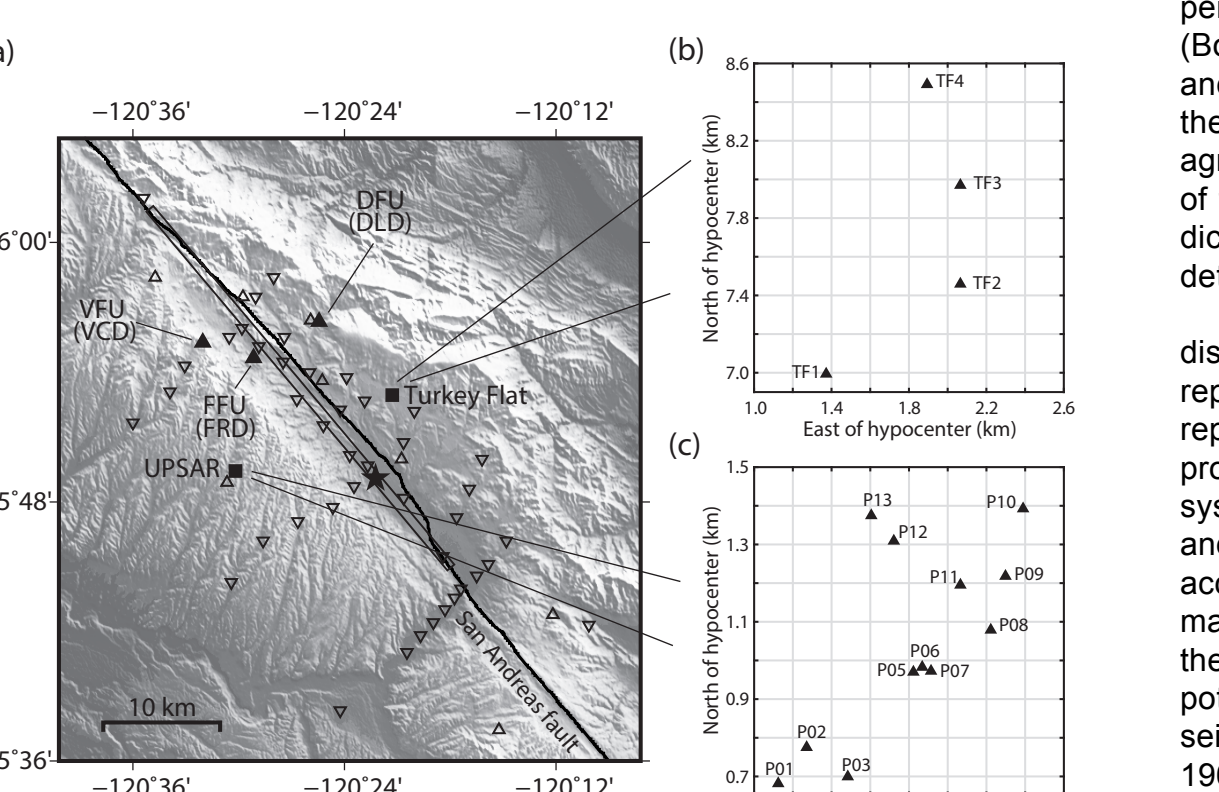


Figure 1. (a) Map of the 2004 Parkfield earthquake, showing the San Andreas fault (thick line), the hypocenter location (star), the surface projection of the fault model proposed by Liu et al. (2006) (rectangle), and the locations of the strong-motion stations. The California Geological Survey (CGS) and USGS GEOS stations are shown as inverted and normal triangles, respectively. The UPSAR and Turkey Flat array (squares) are also shown. In this study, only stations and arrays displayed by filled symbols are considered. Stations in parentheses denote the co-located borehole volumetric strainmeters. (b) Map of the Turkey Flat array stations. (c) Map of the UPSAR stations.

3. Numerical Simulation

Using the fault and crustal models proposed by Liu et al. (2006), a forward ground-motion simulation of the 2004 Parkfield earthquake is performed using a kinematic modeling approach, and synthetic translational motions, strains, and rotations are generated for the selected stations and arrays.

3.1 Fault Model

The fault model proposed by Liu et al. (2006) is based on the kinematic inversion of strong-motion recordings of 43 near-fault stations.

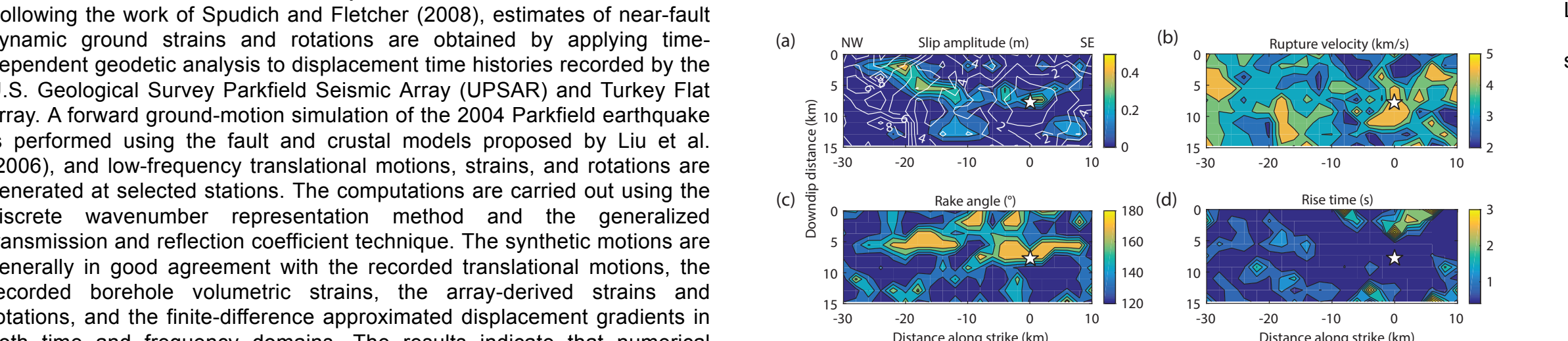


Figure 2. Fault model of the 2004 Parkfield earthquake inferred by Liu et al. (2006): (a) slip amplitude (m) and rupture time (white lines are 1 s contours), (b) rupture velocity (km/s), (c) rake angle (°), and (d) rise time (s). The hypocenter is denoted by the white star.

3.2 Crustal Model

Table 1. 1-D Bilateral Crustal Model for the Parkfield Region (from Liu et al., 2006).

Thickness (km)	Southwest Side			Northeast Side		
	V_p (km/s)	V_s (km/s)	Density (kg/m³)	Q_p	Q_s	Thickness (km)
1.0	1.9	1.0	2000	70	35	0.7
1.0	3.4	2.3	2300	210	0.7	3.8
1.0	4.6	2.4	2300	450	200	0.6
1.0	5.1	3.1	2700	500	350	1.6
1.4	5.6	3.6	2700	550	350	4.0
13.3	6.3	3.6	2800	600	350	6.7
≈	6.8	3.6	2800	680	360	6.2
				4.1	6.8	3.8
				4.1	6.8	3.8
				2.0	2800	650
				350		
				≈	7.0	4.0
						400

3.3 Methodology

The computation of the translational motions, strains, and rotations is performed using the discrete wavenumber representation method (Bouchon and Aki, 1977; Bouchon, 1979). The generalized transmission and reflection coefficient technique (Luco and Apsel, 1983) is utilized for the propagation of the seismic wavefield through the 1-D crustal model. In agreement with the slip inversion of Liu et al. (2006), the frequency range of the simulated ground motions is from 0.16 to 1.0 Hz with the lower limit dictated by the capability of the analog stations and the upper limit determined by the band of applicability of the Green's functions.

In what follows, a brief description of the computation of ground displacements, strains, and rotations using the discrete wavenumber representation method is provided. The basic idea of the method is to represent the elastic wavefield by a superposition of plane waves propagating in discrete directions. Assuming a Cartesian coordinate system in which the x and y axes are normal and parallel to the fault strike and the z axis is along the vertical direction, the displacement vector – according to the Helmholtz's decomposition theorem for vector fields – may be resolved into the gradient of a scalar displacement potential and the curl of a vector displacement potential (with the displacement potentials being the solutions of the wave equations). By representing the seismic dislocations by their body-force equivalents (Burridge and Knopoff, 1964) and following the procedure proposed by Bouchon (1979), the discrete representation of the displacement potentials (or, equivalently, of the displacement and stress vectors) in the wavenumber domain is obtained. Once the ground displacements have been calculated, the computation of the corresponding spatial gradients of displacement (and subsequently the computation of strains and rotations) in the wavenumber domain is carried out using the approach proposed and applied by Bouchon and Aki (1982).

Namely, the discrete representation of the elements of the displacement gradient tensor G in the wavenumber domain can be expressed as a function of the components of the displacement vector, $\mathbf{u} = (u_x, u_y, u_z)^T$, and the stress vector, $\sigma = (\sigma_{xx}, \sigma_{yy}, \sigma_{zz})^T$:

$$G = \begin{bmatrix} \frac{\partial u_x}{\partial x} & \frac{\partial u_x}{\partial y} & \frac{\partial u_x}{\partial z} \\ \frac{\partial u_y}{\partial x} & \frac{\partial u_y}{\partial y} & \frac{\partial u_y}{\partial z} \\ \frac{\partial u_z}{\partial x} & \frac{\partial u_z}{\partial y} & \frac{\partial u_z}{\partial z} \end{bmatrix} = \begin{bmatrix} -ik_x u_x - ik_y u_x & \frac{\sigma_{zx} + ik_x u_z}{\mu} \\ -ik_x u_y - ik_y u_y & \frac{\sigma_{zy} + ik_y u_z}{\mu} \\ -ik_x u_z - ik_y u_z & \frac{\sigma_{xz} + i\lambda + 2\mu}{\lambda + 2\mu} (k_x u_x + k_y u_y) \end{bmatrix}$$

where k_x and k_y are the two horizontal wavenumbers, λ and μ are the Lamé constants, and i is the imaginary unit.

The displacement gradient tensor G can be resolved into a symmetric strain tensor ε and an antisymmetric rotation tensor ω :

$$\varepsilon = \begin{bmatrix} \frac{\partial u_x}{\partial x} & \frac{1}{2}(\frac{\partial u_x}{\partial y} + \frac{\partial u_x}{\partial z}) & \frac{1}{2}(\frac{\partial u_x}{\partial z} + \frac{\partial u_x}{\partial y}) \\ \frac{1}{2}(\frac{\partial u_y}{\partial x} + \frac{\partial u_y}{\partial z}) & \frac{\partial u_y}{\partial y} & \frac{1}{2}(\frac{\partial u_y}{\partial x} + \frac{\partial u_y}{\partial z}) \\ \frac{1}{2}(\frac{\partial u_z}{\partial x} + \frac{\partial u_z}{\partial y}) & \frac{1}{2}(\frac{\partial u_z}{\partial y} + \frac{\partial u_z}{\partial x}) & \frac{\partial u_z}{\partial z} \end{bmatrix} = \begin{bmatrix} \varepsilon_{xx} & \varepsilon_{xy} & \varepsilon_{xz} \\ \varepsilon_{yx} & \varepsilon_{yy} & \varepsilon_{yz} \\ \varepsilon_{zx} & \varepsilon_{zy} & \varepsilon_{zz} \end{bmatrix}$$

$$\omega = \begin{bmatrix} \frac{1}{2}(\frac{\partial u_x}{\partial y} - \frac{\partial u_x}{\partial z}) & \frac{1}{2}(\frac{\partial u_x}{\partial z} - \frac{\partial u_x}{\partial y}) & 0 \\ \frac{1}{2}(\frac{\partial u_y}{\partial x} - \frac{\partial u_y}{\partial z}) & 0 & \frac{1}{2}(\frac{\partial u_y}{\partial z} - \frac{\partial u_y}{\partial x}) \\ 0 & \frac{1}{2}(\frac{\partial u_z}{\partial x} - \frac{\partial u_z}{\partial y}) & 0 \end{bmatrix} = \begin{bmatrix} \omega_x & 0 & \omega_z \\ 0 & \omega_y & 0 \\ 0 & 0 & 0 \end{bmatrix}$$

4. Observations vs. Synthetics

4.1 Translational Motions

Spudich and Fletcher (2008) obtained dynamic ground strains and rotations at the UPSAR array using the seismogeodetic method (Spudich et al., 1995). This method is also used in this study to estimate dynamic ground strains and rotations at the Turkey Flat array.

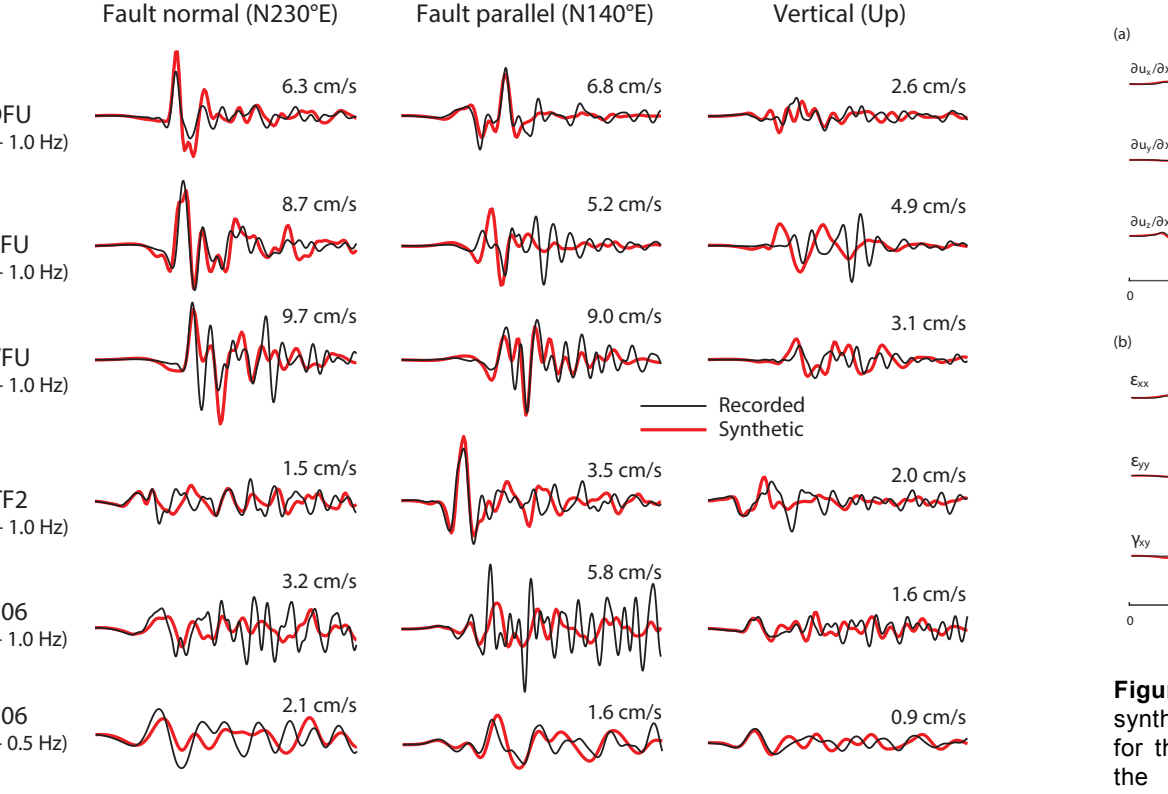


Figure 5. Comparison of (a) recorded and synthetic volumetric strain time histories and (b) corresponding Fourier amplitude spectra for stations DLD, FRD, and VCD. All time histories have been band-pass filtered between 0.16 and 1.0 Hz.

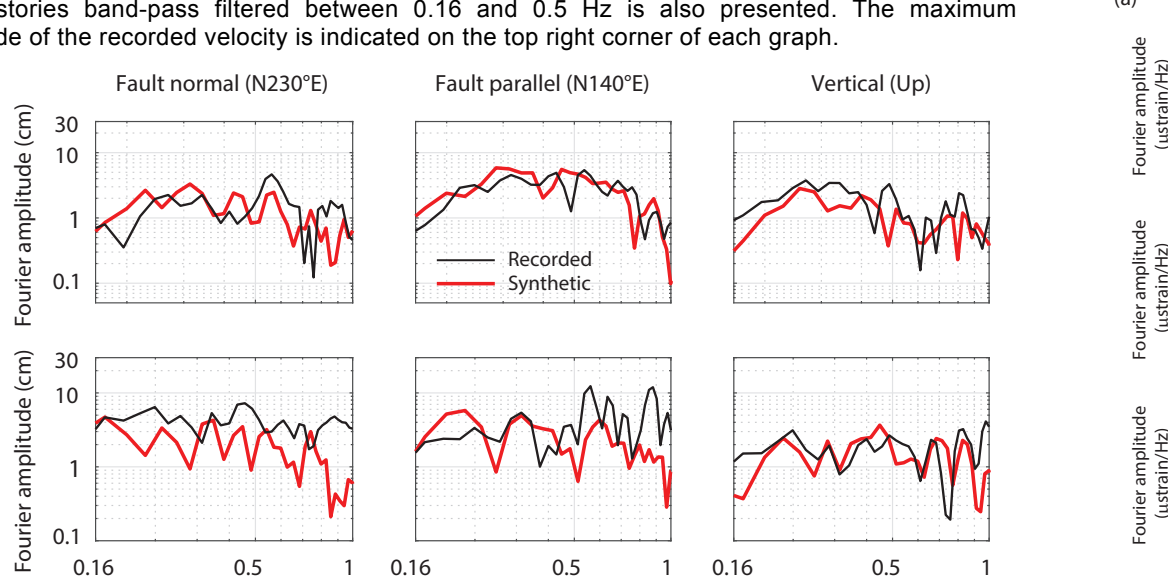


Figure 6. (a) Comparison of array-derived and synthetic displacement gradient time histories for the UPSAR. The x , y and z axes denote the fault-normal ($N230^\circ E$), fault-parallel ($N140^\circ E$), and vertical (up) directions, respectively. All time histories have been band-pass filtered between 0.16 and 1.0 Hz, except that for station P06 the comparison of time histories band-pass filtered between 0.16 and 0.5 Hz is also presented. The maximum amplitude of the recorded velocity is indicated on the top right corner of each graph. (b) Same as (a), except that all time histories are band-pass filtered between 0.16 and 0.5 Hz.

Figure 7. Same as Figure 6, except that all time histories are band-pass filtered between 0.16 and 0.5 Hz.

4.2 Volumetric Strains

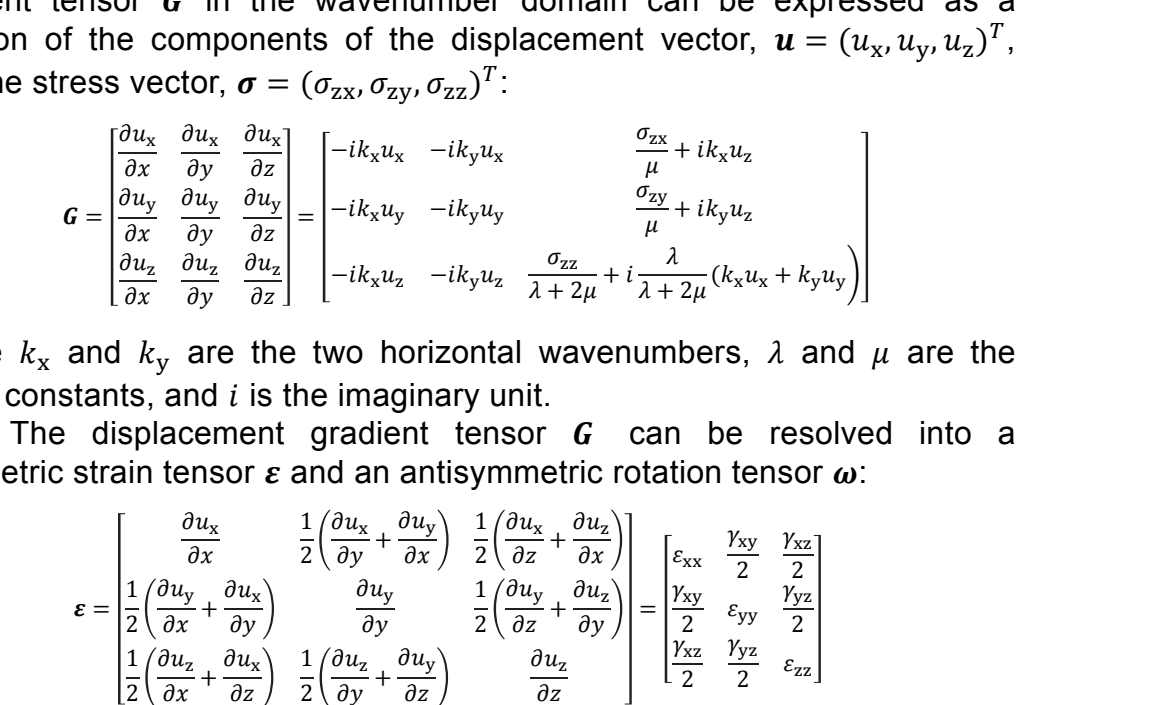


Figure 8. Comparison of Fourier amplitude spectra of recorded and synthetic velocities for stations TF2 and P06. (a) Displacement gradients, (b) strains, and (c) rotations.

4.3 Array-Derived Motions

The displacement gradient tensor G can be resolved into a symmetric strain tensor ε and an antisymmetric rotation tensor ω :

$$\varepsilon = \begin{bmatrix} \frac{\partial u_x}{\partial x} & \frac{1}{2}(\frac{\partial u_x}{\partial y} + \frac{\partial u_x}{\partial z}) & \frac{1}{2}(\frac{\partial u_x}{\partial z} + \frac{\partial u_x}{\partial y}) \\ \frac{1}{2}(\frac{\partial u_y}{\partial x} + \frac{\partial u_y}{\partial z}) & \frac{\partial u_y}{\partial y} & \frac{1}{2}(\frac{\partial u_y}{\partial x} + \frac{\partial u_y}{\partial z}) \\ \frac{1}{2}(\frac{\partial u_z}{\partial x} + \frac{\partial u_z}{\partial y}) & \frac{1}{2}(\frac{\partial u_z}{\partial y} + \frac{\partial u_z}{\partial x}) & \frac{\partial u_z}{\partial z} \end{bmatrix} = \begin{bmatrix} \varepsilon_{xx} & \varepsilon_{xy} & \varepsilon_{xz} \\ \varepsilon_{yx} & \varepsilon_{yy} & \varepsilon_{yz} \\ \varepsilon_{zx} & \varepsilon_{zy} & \varepsilon_{zz} \end{bmatrix}$$

$$\omega = \begin{bmatrix} \frac{1}{2}(\frac{\partial u_x}{\partial y} - \frac{\partial u_x}{\partial z}) & \frac{1}{2}(\frac{\partial u_x}{\partial z} - \frac{\partial u_x}{\partial y}) & 0 \\ \frac{1}{2}(\frac{\partial u_y}{\partial x} - \frac{\partial u_y}{\partial z}) & 0 & \frac{1}{2}(\frac{\partial u_y}{\partial z} - \frac{\partial u_y}{\partial x}) \\ 0 & \frac{1}{2}(\frac{\partial u_z}{\partial x} - \frac{\partial u_z}{\partial y}) & 0 \end{bmatrix} = \begin{bmatrix} \omega_x & 0 & \omega_z \\ 0 & \omega_y & 0 \\ 0 & 0 & 0 \end{bmatrix}$$

The displacement gradient tensor G can be resolved into a symmetric strain tensor ε and an antisymmetric rotation tensor ω :

$$\varepsilon = \begin{bmatrix} \frac{\partial u_x}{\partial x} & \frac{1}{2}(\frac{\partial u_x}{\partial y} + \frac{\partial u_x}{\partial z}) & \frac{1}{2}(\frac{\partial u_x}{\partial z} + \frac{\partial u_x}{\partial y}) \\ \frac{1}{2}(\frac{\partial u_y}{\partial x} + \frac{\partial u_y}{\partial z}) & \frac{\partial u_y}{\partial y} & \frac{1}{2}(\frac{\partial u_y}{\partial x} + \frac{\partial u_y}{\partial z}) \\ \frac{1}{2}(\frac{\partial u_z}{\partial x} + \frac{\partial u_z}{\partial y}) & \frac{1}{2}(\frac{\partial u_z}{\partial y} + \frac{\partial u_z}{\partial x}) & \frac{\partial u_z}{\partial z} \end{bmatrix} = \begin{bmatrix} \varepsilon_{xx} & \varepsilon_{xy} & \varepsilon_{xz} \\ \varepsilon_{yx} & \varepsilon_{yy} & \varepsilon_{yz} \\ \varepsilon_{zx} & \varepsilon_{zy} & \varepsilon_{zz} \end{bmatrix}$$

$$\omega = \begin{bmatrix} \frac{1}{2}(\frac{\partial u_x}{\partial y} - \frac{\partial u_x}{\partial z}) & \frac{1}{2}(\frac{\partial u_x}{\partial z} - \frac{\partial u_x}{\partial y}) & 0 \\ \frac{1}{2}(\frac{\partial u_y}{\partial x} - \frac{\partial u_y}{\partial z}) & 0 & \frac{1}{2}(\frac{\partial u_y}{\partial z} - \frac{\partial u_y}{\partial x}) \\ 0 & \frac{1}{2}(\frac{\partial u_z}{\partial x} - \frac{\partial u_z}{\partial y}) & 0 \end{bmatrix} = \begin{bmatrix} \omega_x & 0 & \omega_z \\ 0 & \omega_y & 0 \\ 0 & 0 & 0 \end{bmatrix}$$

The displacement gradient tensor G can be resolved into a symmetric strain tensor ε and an antisymmetric rotation tensor ω :

$$\varepsilon = \begin{bmatrix} \frac{\partial u_x}{\partial x} & \frac{1}{2}(\frac{\partial u_x}{\partial y} + \frac{\partial u_x}{\partial z}) & \frac{1}{2}(\frac{\partial u_x}{\partial z} + \frac{\partial u_x}{\partial y}) \\ \frac{1}{2}(\frac{\partial u_y}{\partial x} + \frac{\partial u_y}{\partial z}) & \frac{\partial u_y}{\partial y} & \frac{1}{2}(\frac{\partial u_y}{\partial x} + \frac{\partial u_y}{\partial z}) \\ \frac{1}{2}(\frac{\partial u_z}{\partial x} + \frac{\partial u_z}{\partial y}) & \frac{1}{2}(\frac{\partial u_z}{\partial y} + \frac{\partial u_z}{\partial x}) & \frac{\partial u_z}{\partial z} \end{bmatrix} = \begin{bmatrix} \varepsilon_{xx} & \varepsilon_{xy} & \varepsilon_{xz} \\ \varepsilon_{yx} & \varepsilon_{yy} & \varepsilon_{yz} \\ \varepsilon_{zx} & \varepsilon_{zy} & \varepsilon_{zz} \end{bmatrix}$$
<